

JRC TECHNICAL REPORTS

Analysis of Intermittent Distributed Connectivity in Urban Areas

Analysis of hypothetical connectivity of wirelessly connected networks and infrastructures deployed over large regions.

Bono F., Gutiérrez E., Renaldi G.

2017



This publication is a Technical report by the Joint Research Centre (JRC), the European Commission's science and knowledge service. It aims to provide evidence-based scientific support to the European policymaking process. The scientific output expressed does not imply a policy position of the European Commission. Neither the European Commission nor any person acting on behalf of the Commission is responsible for the use that might be made of this publication.

Contact information

Name: Eugenio Gutiérrez
Address: CDMA -1/018, Rue Champs de Mars, 21, B-1049 Brussels, Belgium
Email: eugenio.gutierrez@ec.europa.eu

Tel.: +32 2 29 93126

JRC Science Hub

<https://ec.europa.eu/jrc>

JRC109273

EUR 28881 EN

PDF ISBN 978-92-79-76588-9 ISSN 1831-9424 doi:10.2760/02224

Luxembourg: Publications Office of the European Union, 2017
© European Union, 2017

Reuse is authorised provided the source is acknowledged. The reuse policy of European Commission documents is regulated by Decision 2011/833/EU (OJ L 330, 14.12.2011, p. 39).

For any use or reproduction of photos or other material that is not under the EU copyright, permission must be sought directly from the copyright holders.

How to cite this report: Bono F., Gutiérrez E., Renaldi G., Analysis of Intermittent Distributed Connectivity in Urban Areas : Analysis of hypothetical connectivity of wirelessly connected networks and infrastructures deployed over large regions , EUR 28881 EN , European Commission, Luxembourg, 2017, 978-92-79-76588-9, doi:10.2760/02224, PUBSY No.

All images © European Union 2017, except:
Front cover, left frame, and Figures 4 and 5 photogrammetry base images. Source: Google.
Figures 1 and Figure 3. Source: CIRB Brussels UrbIS data sets.

Analysis of Intermittent Distributed Connectivity in Urban Areas

Analysis of hypothetical connectivity
of wirelessly interconnected networks
and infrastructures deployed
over large regions.

JRC Unit E.4

Bono F., Gutiérrez E., Renaldi G.

[This page intentionally left blank]

Table of Contents

1	Introduction	8
2	Structure of the Report	8
3	Data Preparation	9
3.1	Compilation of data for the analysis	11
4	Experimental Range of wireless devices	15
4.1	Cut off range.....	15
4.2	Signal decay	17
5	Analysis of Connectivity.....	17
6	Analysis of intermittency on Percolation Connectivity	24
7	Conclusions and next steps	27
	Bibliography	28

Table of figures

Figure 1 - Brussels spatial data subdivision in 1sqkm tiles (image from Urbis Digital Mapping)10

Figure 2 – ArcGIS model for the creation of wireless communication network based on buildings centroids ...12

Figure 3 - Urban plan showing roads and centroids of building plots [building footprints source: Urbis Digital Mapping, Region Bruxelles].13

Figure 4 - Basic LOS connectivity in tile 149169 with ranges 25m, 50m, 75m, and 100m [Google base image photogrammetry source].....14

Figure 5 - General view of location of nodes in the vicinity of the ELSA laboratory and two generic (not necessarily real) percolation path examples from the source and sink nodes 102 (top left) and 101 (bottom left) respectively [Google base image photogrammetry source].16

Figure 6 - Number of components as function of wireless range19

Figure 7 - Eigenvalue spectrum19

Figure 8 - Connectivity matrix A_{100} for range up to 100 metres20

Figure 9 - Histogram Degree20

Figure 10 - Histogram of full geodesic matrix entries.22

Figure 11 - Histogram of mean geodesic distances between nodes22

Figure 12 - ΣD_{100} (top), ΣA_{100} (centre) and their ratio $\Sigma D_{100} / \Sigma A_{100}$ (bottom) for each node23

Figure 13 - Node size proportional to the connectivity 'remoteness' ratio $\Sigma D_{100} / \Sigma A_{100}$. Some examples of high (N507 and N87) and low (N1023) remoteness are indicated.23

Figure 14 - The success rate may vary considerably from node to node.25

Figure 15 - The effective mean commute distance increases for $p < 1$; longer paths are required because the availability of active nodes in the original shortest paths are inactive25

Figure 16 - Here we show that the average geodesic distance as a function of probability is equivalent to the average of the normalised ones.26

List of tables

Table 1 – Number of connections in tile 149169 based on communication distance11

Table 2 - shows the approximate line-of-sight distance L from node 101 to all others, where it can be seen that the absolute value of the Fiedler eigenvector ψ_f is closely correlated (0.98) to the square of the normalised distance from node 101.....16

Abstract

Analysis of hypothetical connectivity of wirelessly interconnected networks and infrastructures deployed over a one-square kilometre of the Brussels Metropolitan area is presented. Upper and lower margins of wireless transceiver range are considered with a view to characterise representative interconnectivity profiles. Graph and percolation analyses of intermittent connectivity and its implications for resilience and vulnerability of the network are discussed. Based on these findings the report presents a proposal for the dimensioning of connectivity profiles for generic areas based on intrinsic algebraic network properties.

1 Introduction

The viability of networks composed of billions of interconnected sensing and/or computation nodes would, most probably, need to be designed in order to perform in a practically energy-autonomous and maintenance-free state; contrariwise, if these nodes required a regular ubiquitous manual upkeep, many of the advantages or services such networks are purported to provide would be offset by the cost and labour compounded in their maintenance.

Many of the recently proposed, so-called, *techtopias* and future ICT frameworks are reliant on low-cost, low maintenance, wireless communication devices. Although wired systems will still form part of many such networks, wireless systems will, and in some cases already are, more predominant, especially in the remoter parts of the world where standard infrastructures are non-existent. The capital investment required for quality wired infrastructures is prohibitively expensive, whereas that for wireless telephony make it possible for billions of the world's poorest citizens to have access to private cellular telephony where none had thought it possible a generation earlier.

Of course, in addition to its cheaper infrastructure, wireless systems are inherently mobile, which for some cases may be a design prerequisite, such as when accompanying living or inanimate mobile objects, or they may be fortuitously advantageous if, for instance, the location of the device needs to be displaced for some reason. A problem with wireless networks is that, by definition, they will not necessarily have access to a wired energy grid. Moreover, even assuming that nodes are equipped with an energy-harvesting device, the absence of a 'limitless' energy supply puts serious constraints on power usage, of which that used for radio transmission and reception may quickly undermine the node's energy resources (Halgamuge, 2009).

In order to reduce the energy draw, both physical (sophisticated antennas) and algorithmic (communication protocols) approaches have been heavily explored (Anastasi, 2009) (Akkaya, 2003; Zhang, 2012). Because transmission energy goes up with the power of the wireless range, much effort has been devoted to the optimization of multi-hop, peer-to-peer, communication protocols (Morais Cordeiro C., 2011). The question arises as to how best to deploy the networks—set within a geographic context—in order to optimise the overall system performance; this last aspect has been the subject of much development, especially for environmental monitoring in difficult to access locations (Delin, 2005; Larios, 2013) (Nittel, 2009) (Younis, 2007) .

In this paper we study a scenario within the context of an urban area where a wireless sensor network is to be deployed. It is conjectured that the zone selected is sufficiently representative to expand the findings herein to larger areas by assuming a statistical homogeneity of the main characteristics under investigation.

2 Structure of the Report

In the first part of this paper we describe the data preparation for the urban area under study, the compilation of the data sets and, from these, the generation of the graph structure of node-network spanning the area.

The structure of the network consists in associating the location of the transceiver nodes to that of the building plan within the urban structure itself. This selection was made because it coincides with a fundamental layout of the city, which, in turn, is identified with the main thoroughfares. Having established the node locations, we considered how to link the nodes together on the basis of the strength of the transceiver range. In the first instance we make tentative selections of ranges in order to gauge how the network varies for a number of nominal ranges; this provides an indication of the size of the networks produced in terms of number of edges generated and gross coverage.

Having configured the overall geographical and topological characteristics of the network we proceed to establish a key physical component, namely the wireless range. This aspect of our study is important given that it constrains the scope of the analysis by virtue of our wish to establish the shortest range for power consumption whilst keeping the network reasonably connected. We show how we arrive at the range value selected based on the data sets obtained from an experimental campaign conducted by the authors on multi-hop wireless nodes (Gutierrez E., 2016).

For the statistical analysis we take a similar approach to that developed in (Strozzi, 2015) used to study percolation between wirelessly-connected shipping containers in a port scenario. In the first instance we re-visit the issue of the relation of connectivity with wireless range by quantifying how the range actually affects the spectral graph properties and the number of connected components. This quantification allows us to confirm the selection of the actual range (100 metres) used in the statistical analysis.

The statistical analysis starts with a diagnostic regarding the average node degree and structure of the geodesic matrices before proceeding with the percolation analysis (i.e. propagation of multi-hop signals through the network). In the first instance we examine a selection of nodes representative of near and remote locations on the graph; by this we mean not simply geographically remote, but topologically remote by virtue of their overall connectivity.

Having extracted some conclusions about the success rate and commute distances observed for the selected individual nodes, we consider how the overall performance of the graph can be evaluated by proxy from certain ratios of the geodesic and connectivity matrices.

3 Data Preparation

The source data for the model of the city of Brussels are compiled by CIRB Brussels (Region de Bruxelles, 2017), the Brussels Regional Informatics Centre, which has the mission of promotion and guidance in the field of IT for local authorities. Spatial Data of the city of Brussels are available in different formats (*cityGML*, *shp*, *skp*); shapefile was selected for the analysis as it is the native format of ESRI ArcGIS, the tool of choice for our spatial analyses.

For the analysis of wireless communication we consider here the 2D footprints of buildings with nodes located at height above the rooftops, therefore we consider wireless propagation in direct line of sight (LOS) with no shadowed positions of buildings between them.

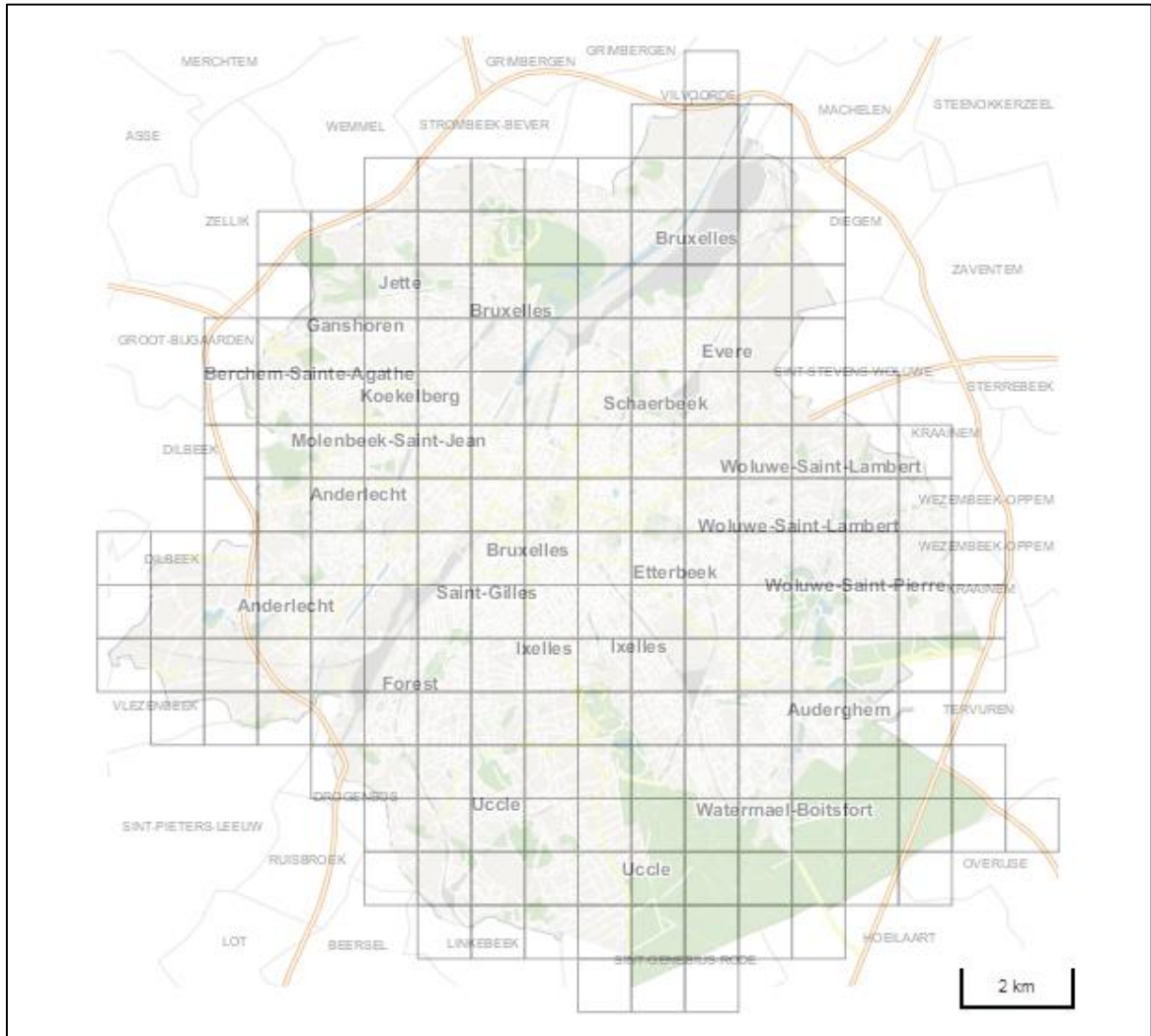


Figure 1 - Brussels spatial data subdivision in 1sqkm tiles
 (image from [Urbis Digital Mapping](#))

Datasets for the city of Brussels are provided in 202 1sqkm-tiles with filenames coded as following:

$$[Datatype]_[long][lat]_[dataset].[extension]$$

As an example, the file *UrbAdm3D_158164_Bu_Ground.shp* contains 3D data of the tile locate in Latitude 164 and *Longitude* 158 with ground footprints of buildings in shapefile format (CIRB Brussels, 11/05/2015).

3.1 Compilation of data for the analysis

Considering one single 1sqkm tile (e.g. the tile 149169 where the JRC Brussels offices are located), we start from the dataset (*UrbAdm3D_149169_Bu_Ground.shp*) of the buildings footprints to generate the basic communication network in *Figure 2*. The feature set is initially duplicated in order to leave the original dataset unchanged. The *[Area]* field is added to the duplicated footprints dataset and each building surface is computed. We then select buildings with an area $\geq 20sqm$ (to discard small premises such as kiosks). To avoid footprints duplication in the analysis (as some of the records contain multiple shapes for the same building with different level of details – LOD) we identify coinciding centroids and discard duplicates.

Centroids are extracted from the single building footprints and their position is computed in terms of *Latitude* and *Longitude*. Sight lines are then generated from every node to every other node, the *[length]* field is added to the dataset and the length of each sight line is computed. It must be noted how this procedure generates self-loops in sight lines. These are eliminated from the sight lines feature set (*NetworkEdges.shp*) as they are not physically meaningful (nodes cannot talk to themselves).

Table 1 – Number of connections in tile 149169 based on communication distance

Distance in [m]	Number of connections
≤ 50	74186
$50 \geq 100$	178210
$100 \geq 150$	266576
$150 \geq 200$	329202

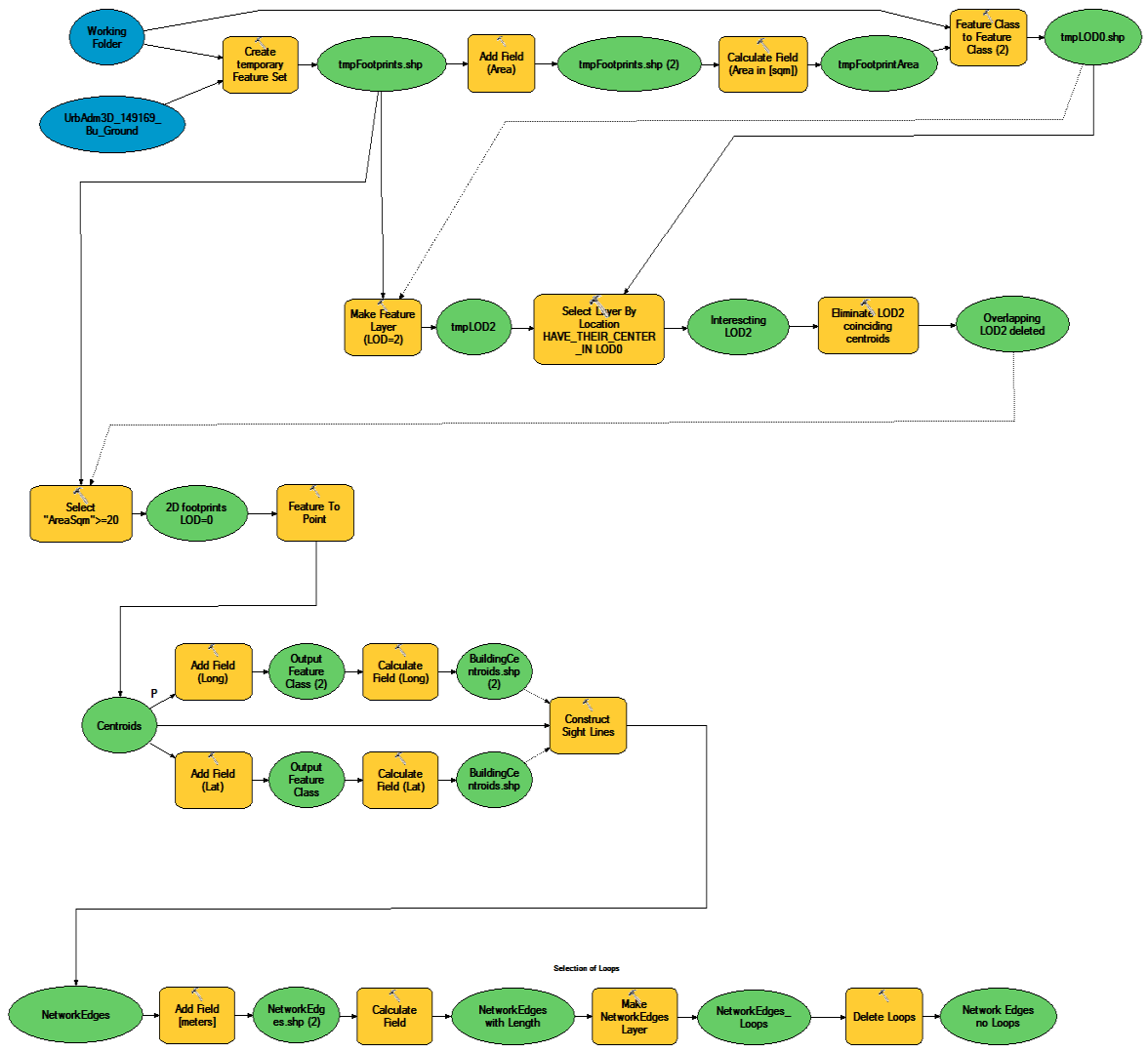
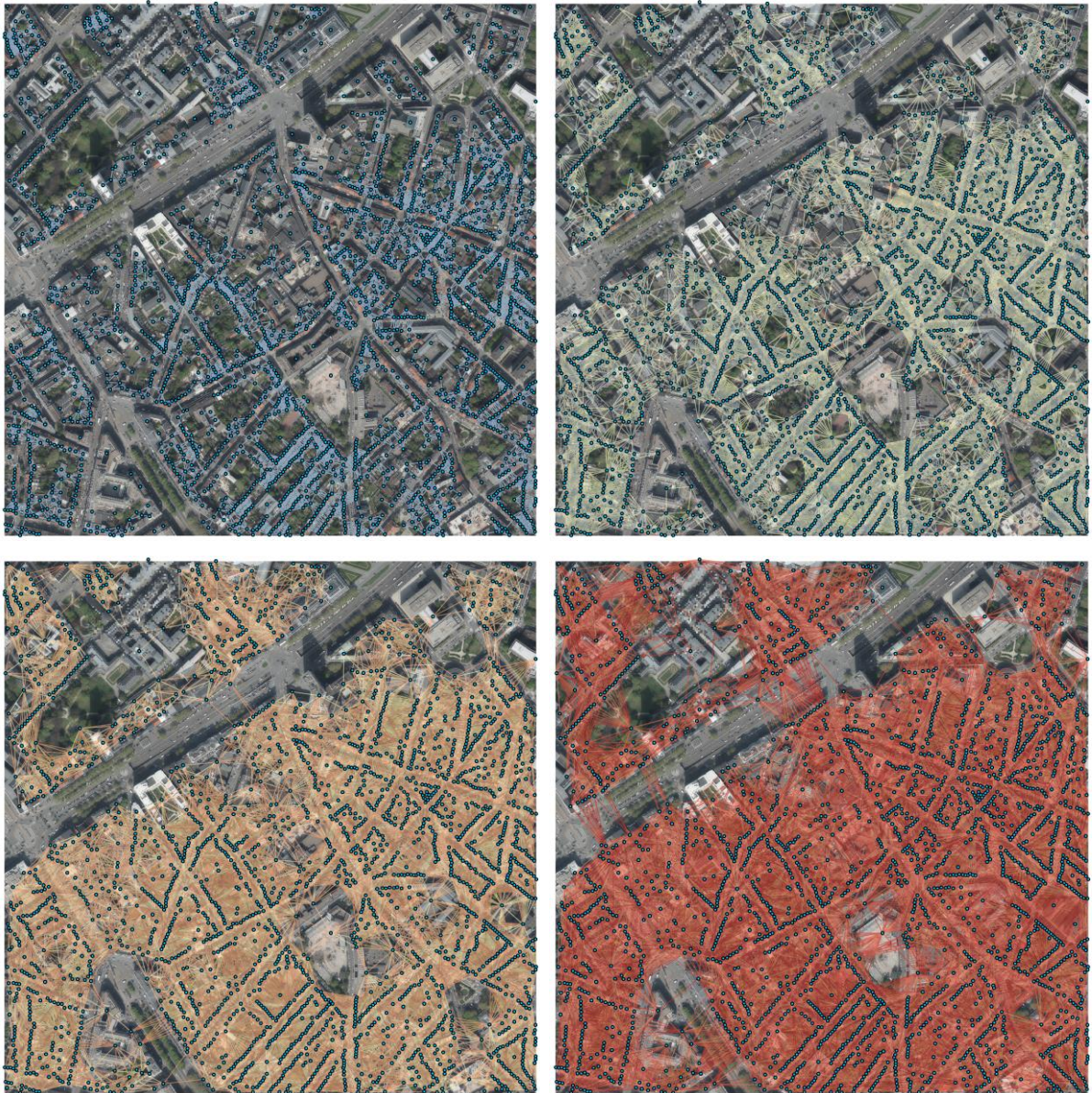


Figure 2 – ArcGIS model for the creation of wireless communication network based on buildings centroids



Figure 3 - Urban plan showing roads and centroids of building plots [building footprints source: UrbiS Digital Mapping, Region Bruxelles].



*Figure 4 - Basic LOS connectivity in tile 149169 with ranges 25m, 50m, 75m, and 100m
[Google base image photogrammetry source]*

4 Experimental Range of wireless devices

The number of network nodes generated by positioning a transceiver node at the area-barycenter of each property results in a network of 2637 vertices. The question now is how to define the connectivity between the nodes of the network.

In principle, within our relatively small selected area, it is technically possible for any two transceiver devices to be wirelessly connected; however, it is presumed that, given the 'low-cost' profile of the system under investigation, it would be counterintuitive to deploy high-end technology to circumvent the problems of weak signal transmission, collision, and noise cancellation that may arise in a low cost low maintenance system.

If it were assumed that the network is fully connected (i.e. every other node is connected to all others) then the connectivity matrix would increase with the square of the node number (for the case of symmetric with no self-connections a total of $N^2 - N$ entries are required in the adjacency matrix for a graph of N nodes).

In order to define a preliminary range for the radio device we have based our proposal on the experimental data based on low cost, short range, wireless field trials reported in (Gutierrez E., 2016). In that report results were presented on the percolation of signals through a forward-only, multi-hop, wireless network. In the field trials, the transceiver stations were deployed over an area of approximately 100x50 m, see (Gutierrez E., 2016) .

The network consisted of seven active nodes of which five (nodes 3,4,5,6, and 9) were used as intermediate hops while the other two (nodes 102 and 101) were the Source and Sink for the datagrams. As can be seen from *Figure 5* the paths have to traverse a heterogeneous terrain via a number of hops between devices; starting from an open air source and then via wooded areas and through the main building hall of the ELSA structural testing laboratory. In addition to these mechanical obstacles, there is considerable electromagnetic background noise generated by a combination of high-voltage electrical devices as well as radio frequency carriers from WiFi and cellular networks inducing EMI that affect optimal radio transmission with the consequence of multiple transmission paths from source to sink.

The field trials consisted in monitoring the success rate, latency, and individual paths taken by percolations starting at node 102 and arriving at node 101 as shown in *Figure 5*. We will use the findings of these trials to arrive at a suitable cut-off distance and signal decay rate that we will then apply to the Brussels network presented above.

4.1 Cut off range

In the analysis of the field trials in (Gutierrez E., 2016) it was shown that there were no single-hop or 2-hop percolations between nodes 101 and 102; more specifically, there are no direct communications from nodes 102, 3, or 5 to node 101. Moreover, it was also noted that all percolations to node 101 arrive either through nodes 4, 6 or 9.

Considering the various percolation paths, it was found that the longest hop distance corresponds to that between nodes 3 to 4, which are separated by about *50m*. On this premise one could set a basis for the upper limit of 50 metres as the typical range and examine how connectivity changes as we vary on either side.

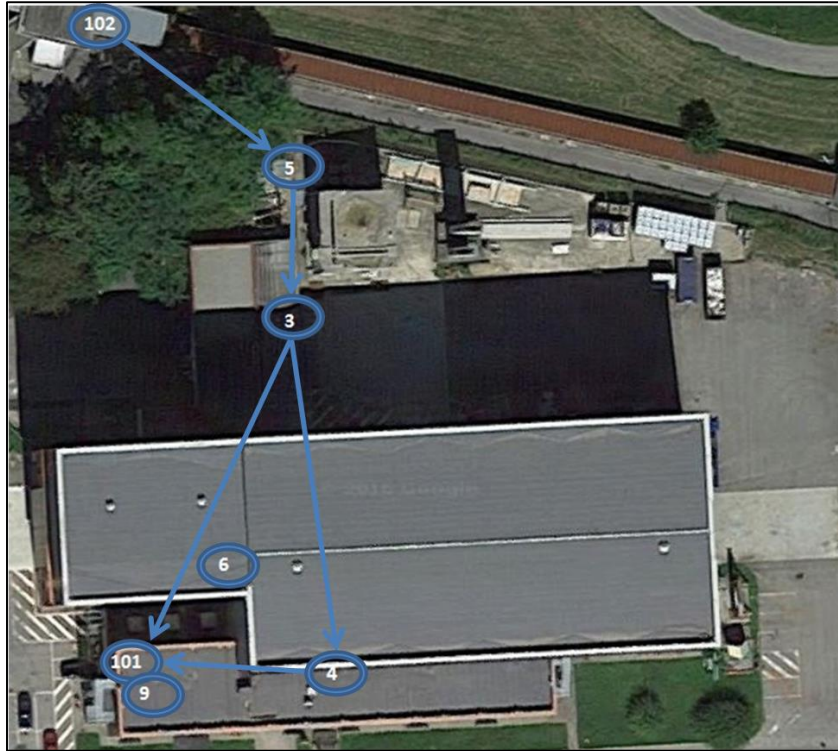


Figure 5 - General view of location of nodes in the vicinity of the ELSA laboratory and two generic (not necessarily real) percolation path examples from the source and sink nodes 102 (top left) and 101 (bottom left) respectively [Google base image photogrammetry source].

Table 2 - shows the approximate line-of-sight distance L from node 101 to all others, where it can be seen that the absolute value of the Fiedler eigenvector ψ_f is closely correlated (0.98) to the square of the normalised distance from node 101.

Node	L (metres)	$(L/L_{\max})^2$	$ \psi_f $
101 (sink)	0	0	0
9	10	0.014	0.015
6	20	0.055	0.097
4	25	0.086	0.126
3	45	0.280	0.241
5	65	0.584	0.515
102 (source)	85	1.0	1.0

4.2 Signal decay

We conjecture that the algebraic connectivity representation of the experimentally-derived percolation matrices can supply an empirical basis of the signal decay. Of particular interest are those experimental paths consisting of five hops, as these imply that during the course of many percolations, we will be able to obtain a statistical description of how the datagram traverses all the available transceiver nodes. We conjecture that this can be used for defining a representative range, and whether it can be correlated to physical deployment location of the devices.

The reasoning is that irrespective of the duty cycle duration (i.e. the proportion of time the transceiver is active) the probability of hopping from one node to another will depend on the signal strength which we have just correlated to the approximate, plan-view, distances between the nodes. Based on this assumption one can fit the spectral properties of the percolation matrices to a distance decay power-law and, having substantiated an empirical decay law, we can then apply it to the Brussels area under investigation.

We examined the compounded matrices for 5-hop percolations. Such percolations will, for a statistically significant number of trials, result in visitations of datagrams for all the intermediate nodes between 102 and 101. In order to discover the most fundamental modes of how datagrams flood the network, we resort to an analogy with mechanical oscillations, whereby the fundamental mode of the Laplacian of the percolation matrix is decomposed into its oscillation spectra. We propose that the, so-called, Fiedler mode (the lowest non-zero eigenvalue mode) governs the flow from the source to the sink nodes of the 5-hop connectivity matrix.

We first composed the agglomerated percolation matrix of all 5-hop paths for 100, 95, 90, 85, 80 and 70 percent duty cycles. For each case we generated the weighted-directed graph Laplacian L (Chung, 1997). We note that we have generated the Laplacian from the directed input degree matrix (as opposed to outputs) into each node; hence the degree of the Source node is zero and that of the Sink node is the value of the total datagrams that have successfully percolated.

Although the Laplacian so obtained is asymmetric, its spectral properties were found to be real. Now, whereas all symmetric matrices exhibit real-valued spectral properties it is not impossible for asymmetric matrices also to have real eigenvalues (for example the product $M^{-1}K$ where M and K are the mass and linear stiffness matrices of discrete mechanical systems, is asymmetric but always has real-valued spectra).

5 Analysis of Connectivity

In Figure 6 it can be seen how the range of the wireless system affects the connectivity of the area covered. Connectivity is expressed in terms of number of connected components shown in log scale versus the range. For a range of 10 metres there are nearly nine-hundred individual components (some of which may be single, isolate, nodes), whereas for a range of approximately 75 metres there is one single connected component. Within this range, it is clear from *Figure 6* that the number of components is reduced exponentially as shown by the approximate overall linear slope of the order of 0.05.

From the same figure it can be seen that between the ranges of 50 to 60 metres there is a change in slope; we conjecture that this is due to the large connectivity barrier introduced by the large separation between two blocks at either side of the main thoroughfare running diagonally along the top half of the area. When the range is sufficiently large it is possible to completely join up the two large blocks: this happens somewhere between 70 and 75 metre range approximately.

Another way of studying the connectivity is to examine the spectrum—eigenvalues—of the graph Laplacian, as shown in Figure 7, where we have plotted the spectrum of the graph Laplacian for wireless ranges of ten to one-hundred metres in five metre increments. It is a well-known property of graph spectra that the number of zero eigenvalues of the Laplacian provides the number of constituent graph components (Chung, 1997).

Upon examination of Figure 7, one can note that as the range is increased, the respective eigenvalue curves intercept the abscissa closer and closer to the origin; thus the ten-metre curve intercepts the abscissa at eigenvalue 841, whereas for the 100 m range the intercept is at 1. This is consistent with the data in Figure 6 which indicated that at $R=100\text{m}$ the number of components is just one; however, the lowest range at which we get full connectivity is for $R=75$ (given a range resolution of ± 5 metres).

For the purpose of our analysis we have chosen a wireless range of 100 metres which results in the connectivity matrix A_{100} with a population density as shown in Figure 8. The A_{100} matrix is far from full; i.e. it is not a fully connected network. Indeed, one can see from the blow-up image that what appear to be dense blocks are in fact sparsely populated; to be precise there are 252386 entries (dots), which, due to symmetry, correspond to 126193 edges—consider that a fully connected network, without self-loops, would generate 3475566 edges or $2,636 \times 2,637 = 6,951,132$ entries.

The average node degree is 95.7; with Node 507 having the lowest degree=9, and the highest being Node 1919 with degree=186. In Figure 9 we show the histogram for the degree distribution from which it can be seen that most nodes have a degree ranging from 40-120, so although the network is far from fully connected, it would indicate that even substantially reducing the effective node duty cycle, enough nodes would remain active to provide sufficient coverage to keep the network connected.

Another important characteristic concerns the geodesic distance matrix D_{100} calculated from the corresponding connectivity matrix A_{100} . In view of the fact that A_{100} is strongly connected (i.e. a path of arbitrary length exists between every node in the network), D_{100} is a full matrix.

Whereas D_{100} provides information of all the shortest paths between all nodes, it does not provide explicit information as to how many distinct shortest paths exist between any two nodes. This is an important consideration when the graph is eroded because we may find that, having eliminated one path possibility, many other commute options may be available in their place; for example a Manhattan type grid provides many commute options between distant nodes, hence we expect the geodesic matrix for such networks to be less sensitive to random erosion than other types of graphs where path multiplicity is not as abundant.

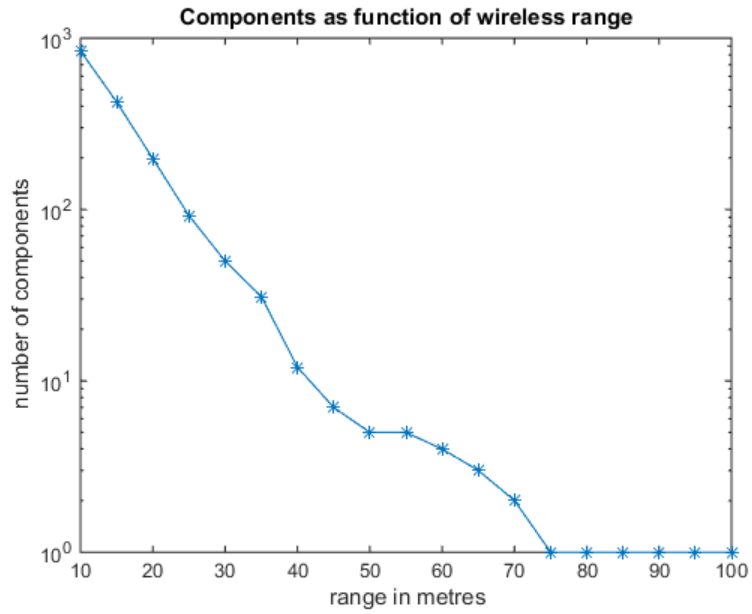


Figure 6 - Number of components as function of wireless range

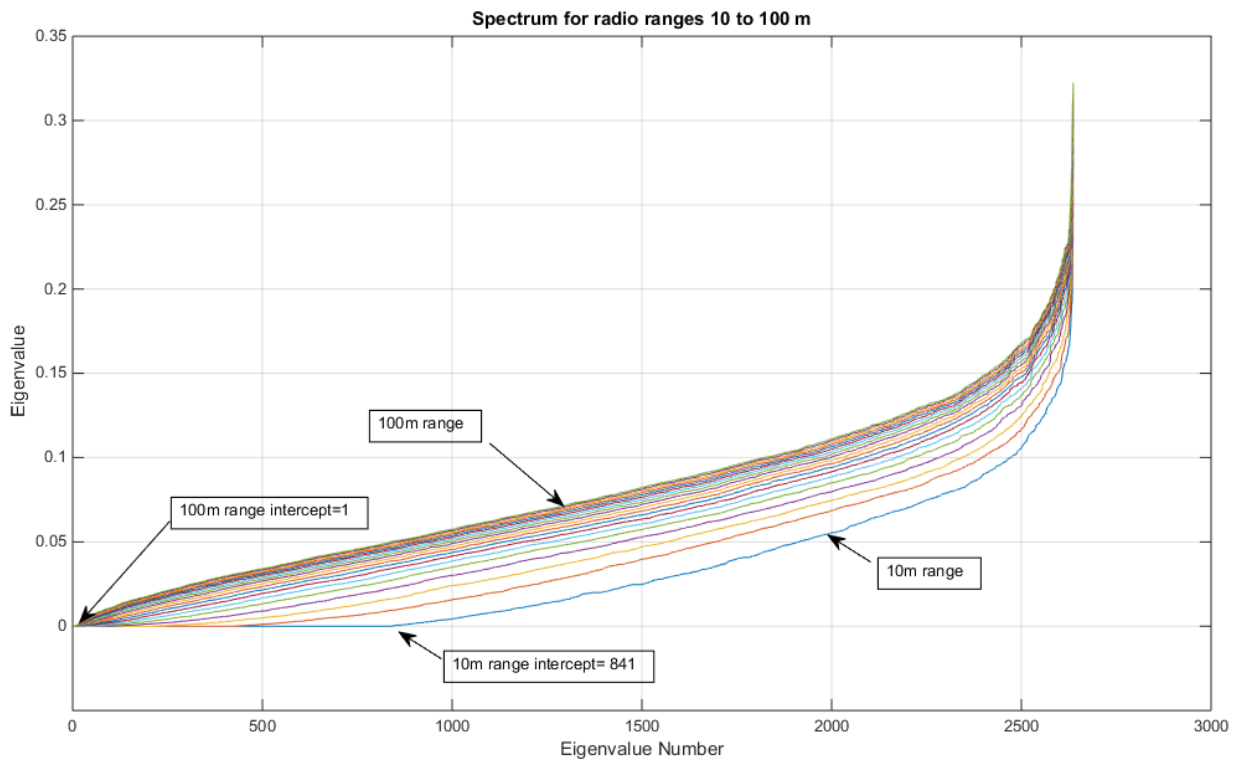


Figure 7 - Eigenvalue spectrum

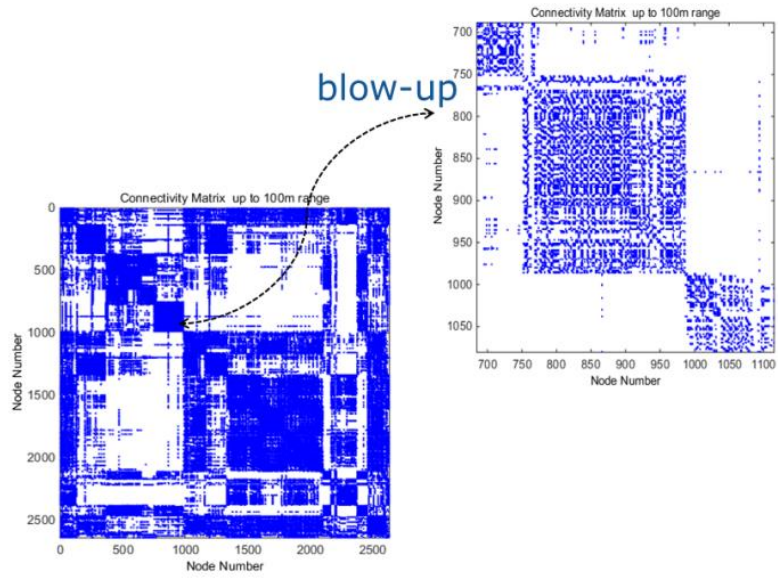


Figure 8 - Connectivity matrix A_{100} for range up to 100 metres

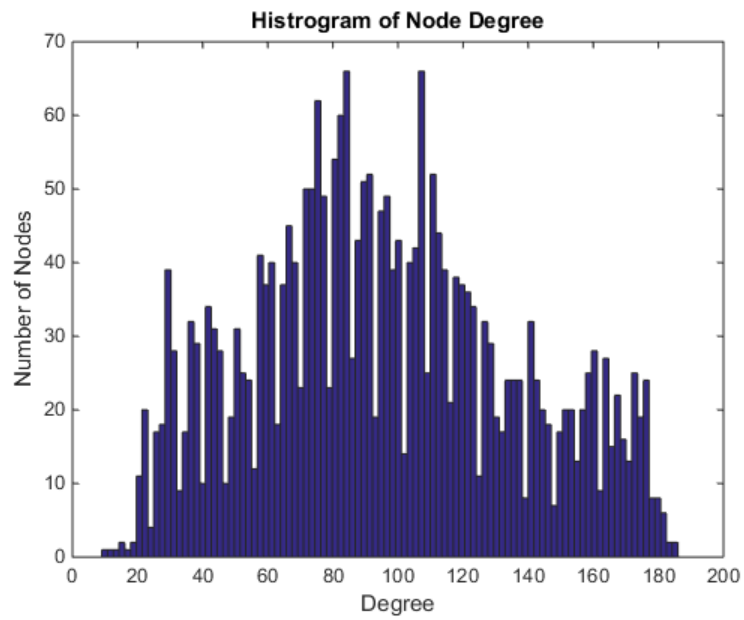


Figure 9 - Histogram Degree

The Geodesic matrix D_{100} provides the unweighted shortest path distances between all nodes, of which the longest of all the shortest paths is known as the graph diameter (which in this case is 17 hops of which there are 12 entries corresponding 6 symmetric path examples). The shortest geodesic is just 1 hop; noting that the Geodesic matrix with entries equal to 1 is simply the connectivity matrix A_{100} . The histogram for the totality of entries of ΣD_{100} is shown in Figure 10 which contains all 6,951,132 entries. Here we see all the dynamic range of the geodesics: from 1 to 17 hops. It can be seen that the histogram is skewed towards the origin (smaller number of hops).

Each row of the 2637 nodes (rows) of the D_{100} matrix has 2636 entries. We now average the entries over each node, condensing these onto a histogram as shown in Figure 11 where we show the mean of the shortest paths for each node. This histogram provides an overview of the statistical lengths of the most probable percolations throughout the network; from here we can see that a random selection of source and sink nodes for a percolation will typically have a path length of the order of 5-6 hops. We shall show how this value comes into play later when we analyse the results from the percolation analysis.

In Figure 12 we have plotted the cumulative Geodesic vector ΣD_{100} (*top frame*) and cumulative Degree vector ΣA_{100} (*middle*) for all nodes and, below, their scalar ratio $\Sigma D_{100} / \Sigma A_{100}$ (also a vector), which we refer to as *remoteness index*. We conjecture that the probability of successful percolation between any two nodes within the network having a certain percentage, p , of active nodes must depend on the length of the available shortest paths—hence the geodesic matrix—and the availability of multiple paths, which is directly the adjacency matrix. In the first instance, when all nodes are active and $p=1$, complete connectivity is assured; but as $p<1$ one finds that, due to the erosion of the connectivity matrix, if a path exists then it will be probably longer than the original. So what happens as $p \ll 1$ and fewer and fewer nodes are available to percolate signals? Well, at some stage there will be so few points that nothing will get through, but however near any two nodes may be, there will be a transition phase where only those nodes close enough to each other will percolate.

So we conjecture that the average percolation commuting distances are, broadly speaking, related to the remoteness index. In Figure 12 we have the confirmation of what was noted in the histograms of Figure 9 to Figure 11 but on a node-by-node basis; what is apparent in the lower frame is that the combination of distance and connectivity tend to highlight the 'remoteness' of some nodes from others, for example Node 507 and Node 87 with a *remoteness index* of 2100 and 1800 approximately, with less remote nodes such as Node 1023 and Node 1956 (corresponding to the JRC CDMA building) with remoteness indices of 87 and 250 respectively.

The *remoteness index* can be mapped directly onto the geographic coordinates of the nodes as shown in Figure 13. Each node's area is in proportion to the diameter whose value is the *remoteness index* vector $\Sigma D_{100} / \Sigma A_{100}$; in addition we have overlaid the mesh of the graph ΣA_{100} onto the same geographical coordinates.

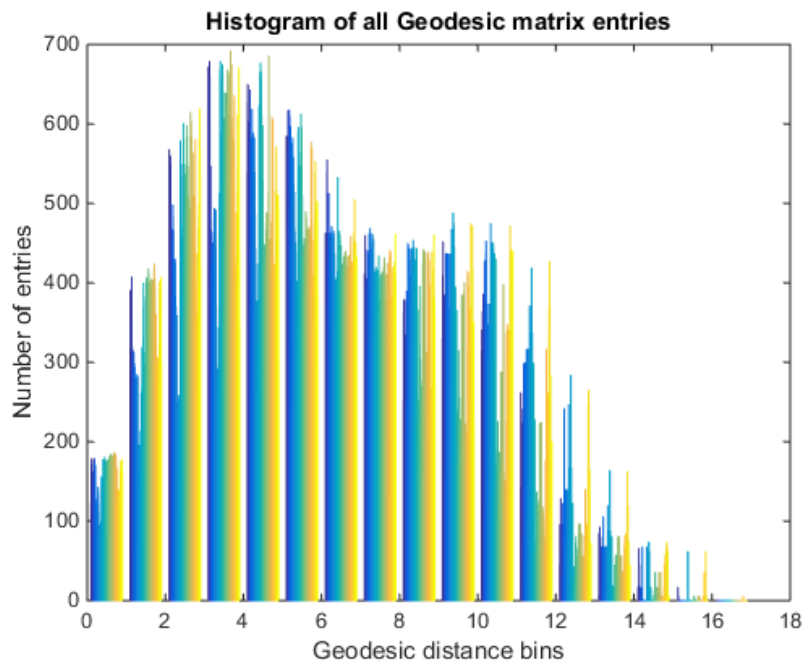


Figure 10 - Histogram of full geodesic matrix entries.

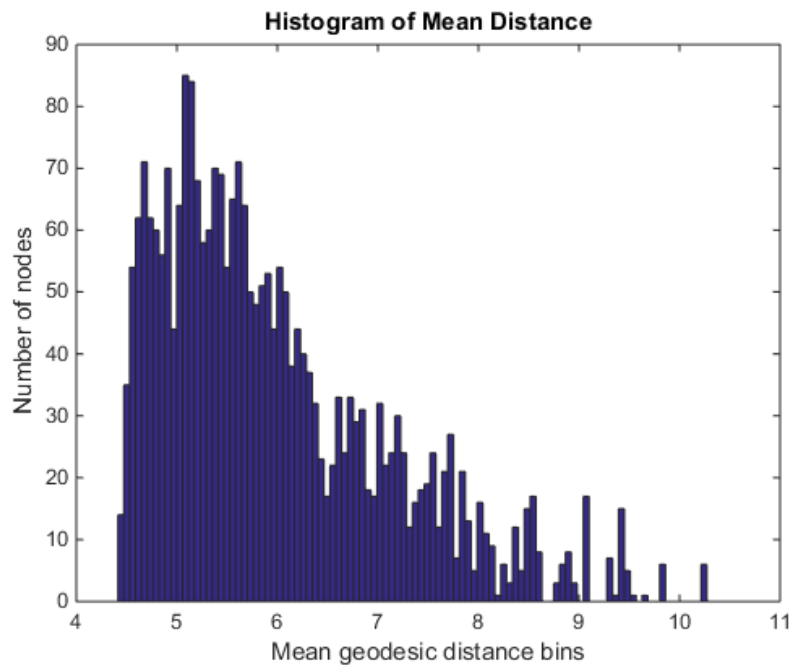


Figure 11 - Histogram of mean geodesic distances between nodes

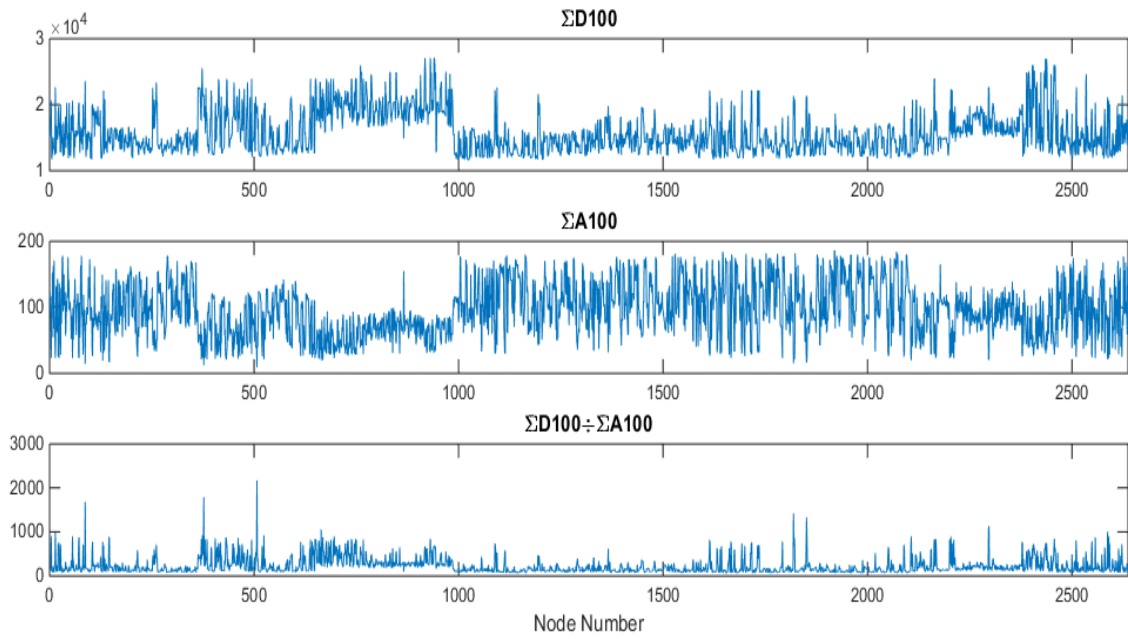


Figure 12 - ΣD_{100} (top), ΣA_{100} (centre) and their ratio $\Sigma D_{100} / \Sigma A_{100}$ (bottom) for each node

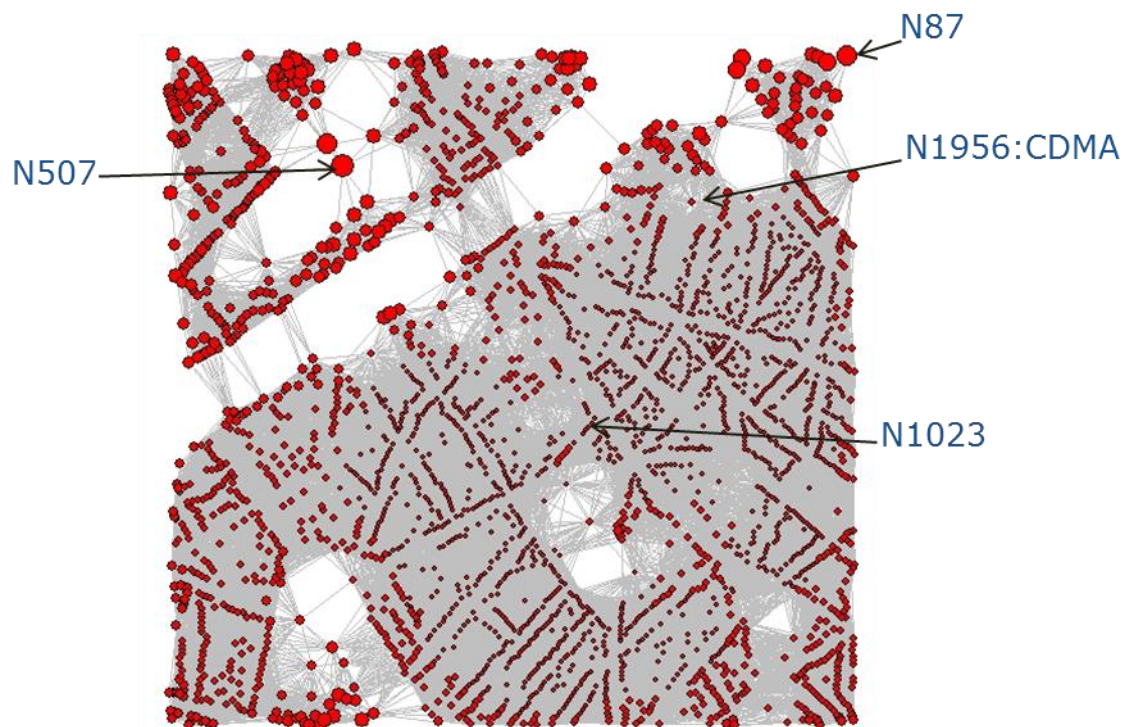


Figure 13 - Node size proportional to the connectivity 'remoteness' ratio $\Sigma D_{100} / \Sigma A_{100}$. Some examples of high (N507 and N87) and low (N1023) remoteness are indicated.

6 Analysis of intermittency on Percolation Connectivity

The following analysis is based on the approaches used in (Strozzi, 2015). We have set up the adjacency and geodesic matrices for the Brussels network based on the individual connectivity links for (unweighted) 100 metre range. Statistical runs are conducted in the following manner: we select some destination buildings (sink nodes) and an assortment of starting points (source nodes) from an arbitrary set of building locations. A *test* consists in looking up matrix D_{100} to read from it the value of the shortest connecting path between a given sink and source pair; this value is referred to as the distance, or commute path, length.

The basis state is given for $p=1$, which is when all the nodes are 'switched on' and capable of communicating with their topological neighbours; this case is trivial as percolation or connectivity is always assured between all nodes. The next aspect to consider is what happens if, for whatever reason (be it due to purposely designed functionality defectiveness) only a proportion, p , of the nodes are active. Clearly, as fewer and fewer nodes become available the percolation of signals, hence connectivity, will not be assured.

In order to measure the performance as p is reduced we define the *Mean Success rate*, p_s , as the total number of occasions when a connecting path between the nodes exists, and the *Mean Commute*, d_m , as the average of the product of the shortest path value times the success rate p_s (i.e. the effected average distance between connected end-to-end nodes). We note that the percentage, p , may be interpreted to indicate the proportion of the nodes that are functionally active, or alternatively, as the proportional duration of the duty cycle during which the node is active.

Each *test* registers, in a case by case manner, if a percolation occurs or a connection exists between the randomly selected source node and a nominated sink node. We repeat the experiments a number of times for each probability and take the average result. On this point we should note that for very low p values, the connectivity may be so reduced as to generate null percolations, thus in order to obtain a meaningful average the number of tests can be adapted to the inverse value of p .

In *Figure 14* we show the success, p_s , rate versus probability, p for a selection of nodes. We have chosen the nodes to represent a range from remote to nearfield nodes (N931, N87, N507, N1956-CDMA and N1023 in that order). The overall trend is that the success rate is at 100% for a wide range of p values; this resilience to fault tolerance (or low levels of duty cycle) is the result of the large average degree of the nodes. At some point the success rate does start to drop off, but its onset varies considerably from one node to another; however, it would appear that nearer nodes N1023 and N1956 exhibit better connectivity than more remote nodes N931, N87 and N507.

In *Figure 15* we show the mean commute length, d_m . In general terms, the effective mean commute distance increases for $p<1$; as the nodes in the original shortest paths (when $p=1$) become inactive, longer paths are required. The more remote the node is, the more accentuated is the commute peak whereas more nearby nodes tend to have flatter commute distances. In other words, remote nodes are less resilient to fault tolerance and require longer commutes, whereas nearfield nodes are more resilient and their average commute paths increase only moderately. In all cases there will be a stage when only very near-neighbours can percolate, hence the sudden drop in the average commute distance for $p\ll 1$.

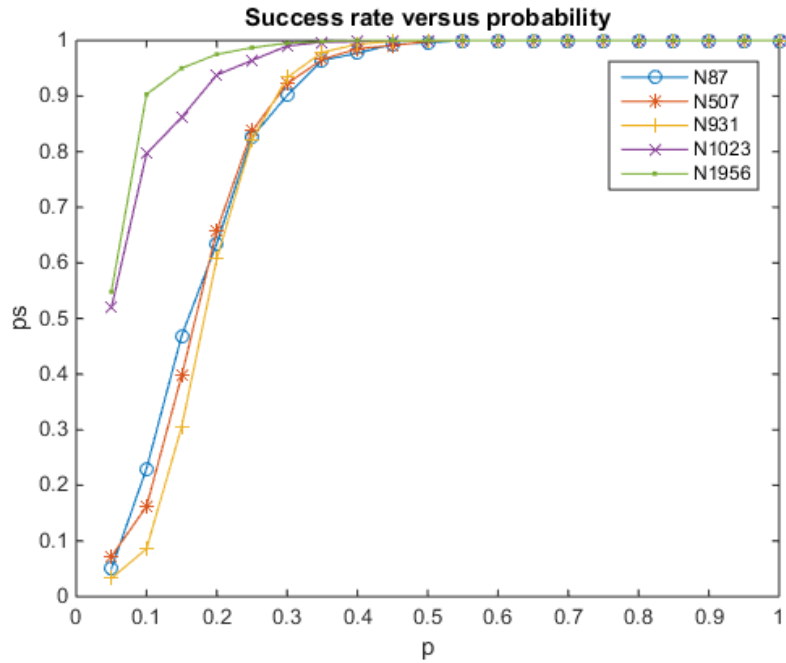


Figure 14 - The success rate may vary considerably from node to node.

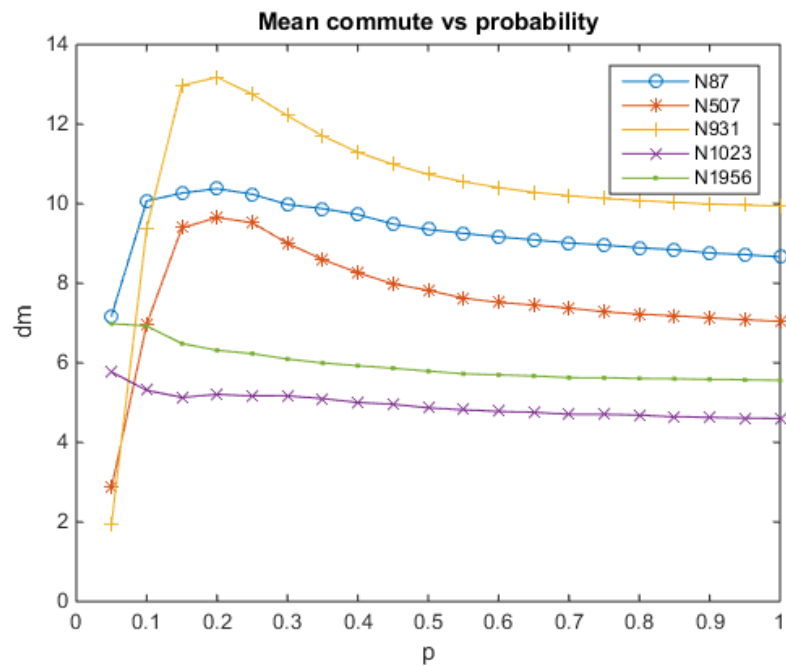


Figure 15 - The effective mean commute distance increases for $p < 1$; longer paths are required because the availability of active nodes in the original shortest paths are inactive

On the basis of the results presented above, another heuristic approach is to compare the profiles of the average of the selected individual notes, to the network-aggregated remoteness measure obtained directly from the connectivity and geodesic matrices. To this purpose we considered the variation of the ratio $\Sigma\Sigma D_{100} / \Sigma\Sigma A_{100}$ (i.e. the summation over all rows and columns of the geodesic and connectivity matrices) as a function of p and normalised by the value of the ratio for $p=1$.

In Figure 16 we present the normalized average of commutes for nodes 1956, 1023, 931, 507 and 87 compared to $\Sigma\Sigma D_{100} / \Sigma\Sigma A_{100}$ from which it appears that the general trend compares well to the average of the small ensemble of individual nodes, especially for the initial part of the curves for $p > 0.4$ and the drop off for $p < 0.1$.

It would appear reasonable, based on these findings, that the average commute distances as a function of p vary in a manner consistent in trend with the ratio $\Sigma\Sigma D_{100} / \Sigma\Sigma A_{100}$; this can provide us with a simple method to quantify the performance of such networks without resorting to numerical simulations for each individual node.

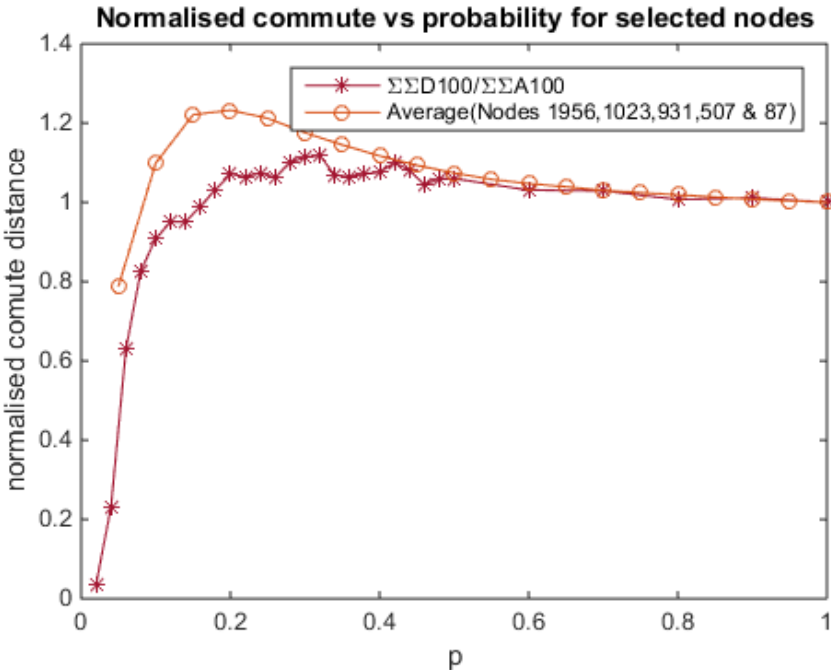


Figure 16 - Here we show that the average geodesic distance as a function of probability is equivalent to the average of the normalised ones.

7 Conclusions and next steps

In this Report we have examined the effects of intermittency on the hypothetical connectivity of a wirelessly interconnected network deployed over an urban environment comprising a one-square kilometre of the Brussels inner Metropolitan area. The network is generated by assigning a transceiver node to the centroid of every building plan within the demarcated area; the wireless transmission range of the nodes is used to establish the number of possible links between nodes. Tentative range trials suggested that the minimum wireless range required to generate a connected network was of the order of 75 metres (corroborated by a variable range spectral graph analysis); although the average distance between nodes (buildings) is much less, barriers to connectivity are introduced by major roads and open spaces such as parks and other public areas.

In order to align the topological connectivity with the practicalities of actual, physical, wireless ranges, we analysed data from an experimental campaign conducted at JRC-Ispra site on smaller-scale networks composed of low-power transceiver nodes. It was concluded that an effective, node-to-node, range of the order of 60 metres is typical for a field scenario not too dissimilar (although perhaps less noisy) to that of the urban area being studied.

Based on this basic network template, percolation analyses were conducted to show how varying levels of node activity result in intermittent connectivity which, in turn, may generate increased latency or disconnection of some parts of the network.

Having studied individual node examples representative of remote and central nodes, we concluded that the ratio of cumulative geodesic and connectivity matrices provides an overall performance *remoteness* measure for the network, and that this measure can be used to ascertain the global commute path profile for percolations in large network.

The next step intends to derive an overall measure for percolation that would allow the amalgamation of large urban networks using agglomerated measures from their component subnetworks. Another area we wish to explore is that of extending our line-of-sight 2D analysis model to one embedded in 3D space, which would include electromagnetic obstacles and interference; for this we intend to adopt fault and attack processes based on node and link intermittency.

Bibliography

- Akkaya, K. Y. (2003). A survey on routing protocols for wireless sensor networks. *3*, 325-349.
- Anastasi, G. C. (2009). Energy conservation in wireless sensor networks: A survey. *Ad Hoc Networks*, *7*, 537-568.
- Chung, F. (1997). *Spectral Graph Theory (CBMS Regional Conference Series in Mathematics)* (Vol. 92). American Mathematical Society.
- CIRB Brussels. (11/05/2015). *Guide de l'utilisateur des produits UrbIS*.
- Delin, K. e. (2005). Environmental studies with the sensor web: Principles and practice. *Sensors*, *5*, 103-117.
- Gutierrez E., R. G. (2016). *Sensor network field trials: validation of signal percolation thorough multiple hops. Studies of physical latency on small-scale networks*. Luxembourg: European Commission.
- Halgamuge, M. Z. (2009). An estimation of sensor energy consumption. *Progress in Electromagnetic Research B*, *12*, 259-295.
- Larios, D. e. (2013). Five years of designing wireless sensor networks in the Doñana biological reserve (spain): An applications approach. *Sensors*, *13*, 12044-12069.
- Morais Cordeiro C., A. D. (2011). *Ad Hoc Sensor Networks: Theory and Applications*. Singapore: World Scientific.
- Nittel, S. (2009). A survey of geosensor networks: Advances in dynamic environmental monitoring. *Sensors*, *9*, 5664-5678.
- Region de Bruxelles. (2017). <http://urbisdownload.gis.irisnet.be/en/temporality>. Retrieved 2017, from UrbIS Digital Mapping CIRB-CIBG .
- Strozzi, F. R. (2015). *Network Segmentation and Spanning Sets, JRC 99540*. Joint Research Centre. Ispra: European Commission.
- Younis, M. A. (2007). Strategies and techniques for node placement in wireless sensor networks: A survey. *Ad Hoc Networks*, *6*, 621-655.
- Zhang, Y. L. (2012). Modelling and energy consumption evaluation of a stochastic wireless sensor network. *EURASIP J. on Wireless Communications and Networking*, *2012*, 282.

GETTING IN TOUCH WITH THE EU

In person

All over the European Union there are hundreds of Europe Direct information centres. You can find the address of the centre nearest you at: <http://europa.eu/contact>

On the phone or by email

Europe Direct is a service that answers your questions about the European Union. You can contact this service:

- by freephone: 00 800 6 7 8 9 10 11 (certain operators may charge for these calls),
- at the following standard number: +32 22999696, or
- by electronic mail via: <http://europa.eu/contact>

FINDING INFORMATION ABOUT THE EU

Online

Information about the European Union in all the official languages of the EU is available on the Europa website at: <http://europa.eu>

EU publications

You can download or order free and priced EU publications from EU Bookshop at: <http://bookshop.europa.eu>. Multiple copies of free publications may be obtained by contacting Europe Direct or your local information centre (see <http://europa.eu/contact>).

JRC Mission

As the science and knowledge service of the European Commission, the Joint Research Centre's mission is to support EU policies with independent evidence throughout the whole policy cycle.



EU Science Hub
ec.europa.eu/jrc



@EU_ScienceHub



EU Science Hub - Joint Research Centre



Joint Research Centre



EU Science Hub



Publications Office

doi: 10.2760/02224

ISBN 978-92-79-76588-9